2007 IEEE International Conference on
Robotics and Automation
Roma, Italy, 10-14 April 2007

Cooperative Standoff Tracking of Uncertain Moving Targets using Active Robot Networks

Eric W. Frew, *Member, IEEE*

***Abstract*—This paper presents a coordination scheme for standoff tracking of an uncertain moving target by cooperating mobile robots with range and bearing sensors. An algorithm is described that transforms a guidance vector field developed for loitering about circular patterns into a vector field that tracks ellipses. Specific elliptical tracking patterns are developed based on the covariance matrix of a stochastic estimation process. Simulation results demonstrate the ability of two aerial robots to coordinate their orbit around an uncertain target moving with constant velocity.**

I. Introduction

ACTIVE sensing in robot networks takes advantage of robot mobility to optimize or improve information gathering activities. For some applications, such as exploration, persistent surveillance, and area coverage, proactive motion and cooperation between multiple vehicles can improve performance in terms of execution time, search efficiency, and system flexibility or robustness. For other applications, such as bearing-only (or range-only) localization and target tracking (Fig. 1), active sensing in terms of single-robot motion or multi-robot collaboration is necessary to provide basic sensing observability.

This paper presents a coordinated control scheme for cooperative stand-off tracking of uncertain moving targets using bearing and range measurements. Standoff tracking consists of following and orbiting around a (possibly moving) target with a specified minimum allowable separation distance. Although originally motivated by cooperative search and tracking of moving ground targets by teams of unmanned aircraft [1], the algorithms presented here apply equally well to tracking applications consisting of unmanned ground vehicles (UGVs), unmanned surface vehicles (USVs), and autonomous underwater vehicles (AUVs).

A key component of active sensing systems is the dependence of information-gathering on robot motion and the ability to predict in advance the effect of robot motion on the quality of information that is collected. For model-based sensing tasks (e.g. feature localization, target tracking, and diffuse target tracking) information-theoretic concepts such as mutual information, Fisher information, and entropy are used to quantify the sensitivity of the sensing task to robot motion and planning algorithms can explicitly formulate sensing objectives in terms of these criteria. Example applications using this approach include: trajectory design to improve bearings-only tracking [2, 3]; path planning to enable a robotic manipulator to grasp a delicate object [4]; target tracking by active sensor networks [5, 6]; collaborative perception by unmanned ground and aerial vehicle teams [7]; vision-based navigation and control [8]; and hierarchical reconnaissance by teams of unmanned aircraft [9].

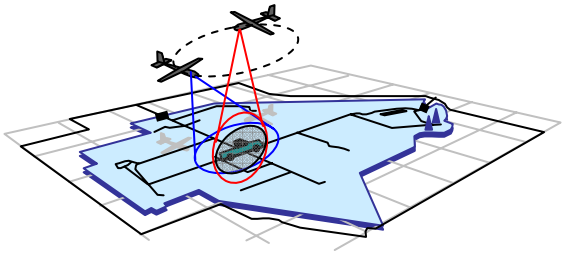

Fig. 1 Cooperative standoff line-of-sight tracking of a moving ground target by two cooperating unmanned aircraft.

An alternative approach to incorporating information-gathering criteria directly into the cooperative control framework is to decompose the problem into a hierarchical structure based on underlying assumptions related to active sensing concepts. For target geo-localization and tracking by cooperating robots, the optimal configuration consists of phased spacing about the target at the minimum allowable stand-off distance [10]. Thus, different tracking algorithms have been designed to coordinate robot motion without explicitly modeling the sensing performance. Control algorithms for the spacing of general oscillators (which can model UAS kinematics) about fixed points have been developed for arbitrary number of agents [11]. The optimal phasing of two UAS orbiting at a fixed radius is used as one of the heuristics in the reconnaissance architecture in Ref. [9]. Cooperative search and tracking of agile targets in the presence of background wind have also been performed by decoupling target assignment and orbit coordination based

Eric W. Frew is an Assistant Professor in the Aerospace Engineerinv Sciences Department at the University of Colorado, Boulder. (phone: 303-735-1285; e-mail: eric.frew@colorado.edu).

on desired phasing between UAS [1, 12].

The optimal coordination algorithms referred to above are designed to minimize the uncertainty of target estimation, but do not incorporate this uncertainty back into the robot motion control. For cooperative standoff geo-localization and target motion estimation by two vehicles, optimal spacing is derived in order to minimize a scalar function of the resulting estimate error covariance matrix. Unfortunately, the coordinated control algorithms then invoke the certainty equivalence principle to derive circular orbit patterns around the current estimate [1, 12]. In order to insure standoff tracking, i.e. that the robot maintains the required separation distance, the orbit patterns must include this uncertainty. For planar estimation problems, this uncertainty leads to elliptical contours of constant probability and motivates the need to orbit elliptical patterns.

The cooperative tracking algorithm presented here assumes some high-level coordination layer assigns individual robots to specific sensing tasks. In this work, the sensing task consists of stand-off tracking of an uncertain moving target using range and bearing sensors. The tracking algorithm described here transforms a guidance vector field with global stability properties developed for loitering about circular patterns [1] into a vector field that tracks ellipses. Specific elliptical tracking patterns are developed based on the covariance matrix of a stochastic estimation process. Cooperative phasing around the ellipse by multiple robots is achieved through differential speed commands.

II. System Models

This work is motivated by tracking applications using unmanned aircraft (UA). Thus, the algorithms presented here assume the mobile robots are equipped with a low-level control system that presents the following 2-D kinematic model to the higher level guidance layer:

$$\begin{aligned} \dot{x} &= u_1 \cdot \cos\psi + W_x \\ \dot{y} &= u_1 \cdot \sin\psi + W_y \\ \dot{\psi} &= u_2 \end{aligned} \tag{1}$$

where $[x, y]^T \in \Re^2$ is the two-dimensional inertial position of the aircraft, $\psi \in [0, 2\pi)$ is the aircraft yaw angle, $[W_x, W_y]^T \in \Re^2$ are the components of the background (horizontal) wind velocity, and $u_i \in U_i \quad i = 1,2$ are the commanded air speed and turning rate, which are constrained to the limits

$$\begin{aligned} U_1 &= \{u_1 \in \Re \mid 0 < v_{\min} \le u_1 \le v_{\max}\} \\ U_2 &= \{u_2 \in \Re \mid |u_2| \le \omega_{\max}\} \end{aligned} . \tag{2}$$

When expressed relative to a point $\mathbf{p}_t = [x_t, y_t]^T$ moving with speed $[\dot{x}_t, \dot{y}_t]^T \in \Re^2$, the kinematic model becomes (see Fig. 2)

$$\begin{aligned} \dot{x}_r &= u_1 \cdot \cos\psi + W_x - \dot{x}_t \\ \dot{y}_r &= u_1 \cdot \sin\psi + W_y - \dot{y}_t \\ \dot{\psi} &= u_2 \end{aligned} . \tag{3}$$

Since the wind velocity and moving target velocity enter Eq. (3) in the same way, it is convenient to consider a "virtual" moving target with velocity $\mathbf{v}_T = [T_x, T_y]^T = [\dot{x}_t - W_x, \dot{y}_t - W_y]^T$. Thus, in the remaining sections of this paper we will refer to a *moving target* with the understanding that it is a virtual one whose velocity comes from the moving ground target and the background wind. Furthermore, the virtual moving target allows us to apply the same kinematic model to different vehicles such as unmanned aircraft and mobile ground robots.

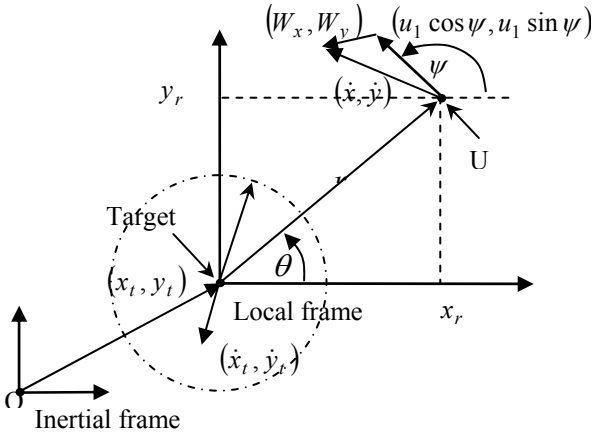

Fig. 2 Tracking geometry with the ground target of interest at the origin of the *local frame*.

Robot guidance is achieved by specifying a desired guidance vector field and using a reference tracking control to follow it. Derivation of guidance vector fields for this application will be described in Section III. The guidance vector field gives the desired velocity which is used to generate the desired heading angle ψ_d and desired turn rate $\dot{\psi}_d$. The heading angle error $e_\psi = \psi - \psi_d$ is driven to zero by the control law

$$u_2 = \dot{\psi}_d - \lambda \cdot (\psi - \psi_d) . \tag{4}$$

which yields a heading angle error rate $\dot{e}_\psi = -\lambda e_\psi$.

Ground target motion is modeled as constant velocity with accelerations acting as process noise. Thus, the equations of motion for the target are

$$\mathbf{x}_t[k+1] = \mathbf{F} \cdot \mathbf{x}_t[k] + \mathbf{G} \cdot \mathbf{w}[k] \tag{5}$$

$$\mathbf{F}=\begin{bmatrix}1 & T_s & 0 & 0\\ 0 & 1 & 0 & 0\\ 0 & 0 & 1 & T_s\\ 0 & 0 & 0 & 1\end{bmatrix}\quad G=\begin{bmatrix}T_s^2/2 & 0\\ T_s & 0\\ 0 & T_s^2/2\\ 0 & T_s\end{bmatrix}$$

where $\mathbf{x}_t=\left[x_t,\dot{x}_t,y_t,\dot{y}_t\right]^t$, $E\left[\mathbf{w}\mathbf{w}^t\right]=\mathbf{Q}_t$.

In this work we consider two-dimensional problems in which the robots know their own locations and are equipped with sensors that measure the bearing angle and range to an obstacle. The measurement is given by

$$\begin{aligned}\mathbf{z}_k &= h\left(\mathbf{x}_k,\boldsymbol{\theta}_k\right)+\mathbf{v}\\ &=\begin{bmatrix}\sqrt{\left(\mathbf{x}_k(1)-\boldsymbol{\theta}_k(1)\right)^2+\left(\mathbf{x}_k(2)-\boldsymbol{\theta}_k(2)\right)^2}\\ \tan^{-1}\left(\dfrac{\mathbf{x}_k(2)-\boldsymbol{\theta}_k(2)}{\mathbf{x}_k(1)-\boldsymbol{\theta}_k(1)}\right)\end{bmatrix}+\mathbf{v}\end{aligned}\qquad(6)$$

where $\boldsymbol{\theta}_k$ is the vector of the 2-D position of the target object and $\mathbf{v}$ is white noise with uncorrelated variances σ_R^2 and σ_θ^2 in the range and bearing measurements respectively. The measurement equation Eq. (14) can describe many different types of sensors. Taking $\sigma_R^2=\infty,\ \sigma_\theta^2<\infty$ models passive non-cooperative (i.e. bearings-only) sensing such as EO/IR cameras or passive sonar. On the other hand, taking $\sigma_R^2<\infty,\ \sigma_\theta^2=\infty$ models pure trilateration, e.g. using some types of radar. Finally, conventional radar systems include both bearing and range measurements and would have finite values for both variances.

III. Tracking Elliptical Contours Using Lyapunov Vector Fields

In this section we describe an algorithm for generating guidance vector fields that follow elliptical contours. The algorithm is based on a Lyapunov vector field approach that leads to a circular loiter pattern [1]. A linear transformation is used to stretch the pattern into an ellipse whose shape can be defined by singular value decomposition of the transformation matrix. We prove stability of the resulting vector field to the ellipse in the case of any nonsingular transformation.

Consider the Lyapunov function $V(\mathbf{x}_r)=\left(r^2-r_d^2\right)^2$, where $r^2=\mathbf{x}_r^T\mathbf{x}_r=(x-x_t)^2+(y-y_t)^2$ is the squared radial distance of the robot from the target. The total time derivative of $V(\mathbf{x})$ is given by

$$\frac{dV}{dt}=\begin{bmatrix}\dfrac{\partial V}{\partial x_r} & \dfrac{\partial V}{\partial y_r}\end{bmatrix}\begin{bmatrix}\dot{x}_r\\ \dot{y}_r\end{bmatrix}\qquad(7)$$

and this can be specified to be non-positive by choosing desired vehicle velocity $\dot{x}_r=\dot{x}_d$ and $\dot{y}_r=\dot{y}_d$ according to the guidance vector field $\mathbf{f}(\mathbf{x}_r)$ given by

$$\mathbf{f}(\mathbf{x}_r)=\begin{bmatrix}\dot{x}_d\\ \dot{y}_d\end{bmatrix}=\alpha\left(\frac{-v_0}{r}\right)\cdot\begin{bmatrix}x_r\cdot\dfrac{r^2-r_d^2}{r^2+r_d^2}+y_r\cdot\dfrac{2rr_d}{r^2+r_d^2}\\ y_r\cdot\dfrac{r^2-r_d^2}{r^2+r_d^2}-x_r\cdot\dfrac{2rr_d}{r^2+r_d^2}\end{bmatrix}\qquad(8)$$

where α is non-negative. This vector field produces the non-positive rate of change of V

$$\frac{dV}{dt}=\frac{-4\alpha v_o r\left(r^2-r_d^2\right)^2}{r^2+r_d^2}.\qquad(9)$$

If α is bounded away from zero, $\dot{V}$ is zero only on the loiter circle $(r=r_d)$ and when $r=0$. This ensures that the vector field produces a globally attractive limit cycle [1]. When r is large compared to r_d, the vector field points to the loiter circle center, but the field veers away when approaching the circle to smoothly entrain the motion into a left turn loiter.

To extend the original Lyapunov vector approach for circular patterns to elliptical ones we prove the following:

Theorem 1: Given the linear transformation $\mathbf{x}'=\mathbf{M}^{-1}\mathbf{x}_r$ where $\mathbf{M}$ is a nonsingular matrix and the vector field $\mathbf{f}(\mathbf{x}_r)$ described by (8) that drives the Lyapunov function $V(\mathbf{x}_r)=\left(r^2-r_d^2\right)^2$ to zero, then the vector field

$$\mathbf{f}'(\mathbf{x}_r)=\mathbf{M}\cdot\mathbf{f}\left(\mathbf{M}^{-1}\mathbf{x}_r\right)\qquad(10)$$

drives the new Lyapunov function

$$V'(\mathbf{x}_r)=V(\mathbf{x}')=\left(r'^2-r_d^2\right)^2\qquad(11)$$

to zero, where $r'^2=\mathbf{x}'^T\mathbf{x}'=\mathbf{x}_r^T\mathbf{M}^{-T}\mathbf{M}^{-1}\mathbf{x}_r$.

Proof: The time rate of change of the new Lyapunov function is

$$\begin{aligned}\frac{dV'}{dt}&=\frac{dV}{d\mathbf{x}'}\cdot\frac{d\mathbf{x}'}{d\mathbf{x}_r}\cdot\frac{d\mathbf{x}_r}{dt}\\ &=\begin{bmatrix}\dfrac{\partial V}{\partial x'} & \dfrac{\partial V}{\partial y'}\end{bmatrix}\cdot\mathbf{M}^{-1}\cdot\dot{\mathbf{x}}_r\end{aligned}\qquad(12)$$

Taking $\dot{x}_r=\mathbf{f}'(\mathbf{x}_r)=\mathbf{M}\cdot\mathbf{f}\left(\mathbf{M}^{-1}\mathbf{x}_r\right)$ yields

$$\begin{aligned}\frac{dV'}{dt}&=\begin{bmatrix}\dfrac{\partial V(\mathbf{x}')}{\partial x'} & \dfrac{\partial V(\mathbf{x}')}{\partial y'}\end{bmatrix}\cdot\mathbf{M}^{-1}\cdot\mathbf{M}\cdot\mathbf{f}(\mathbf{x}')\\ &=\begin{bmatrix}\dfrac{\partial V(\mathbf{x}')}{\partial x'} & \dfrac{\partial V(\mathbf{x}')}{\partial y'}\end{bmatrix}\cdot\mathbf{f}(\mathbf{x}')\end{aligned}\qquad(13)$$

which is equivalent to (7) when substituting $\mathbf{x}'$ for $\mathbf{x}_r$. Thus,

$$\frac{dV'}{dt}=\frac{-4\alpha v_o r'\left(r'^2-r_d^2\right)^2}{r'^2+r_d^2}.\qquad(14)$$

If α is bounded away from zero, $\dot{V}'$ is zero when $r'^2 = r_d^2$. Rewriting this expression reveals the equation for an ellipse $\mathbf{x}_r^T P^{-1} \mathbf{x}_r = r_d^2$ where $P = M^T M$. ☒

Figure 3 shows an example elliptical vector field. This field was generated using (8) with r_d = 1m and matrix

$$\mathbf{M} = \begin{bmatrix} 212.13 & -106.07 \\ 212.13 & 106.07 \end{bmatrix}$$

which generates an ellipse rotated 45 degrees counter-clockwise with major and minor axis of 300m and 150m respectively.

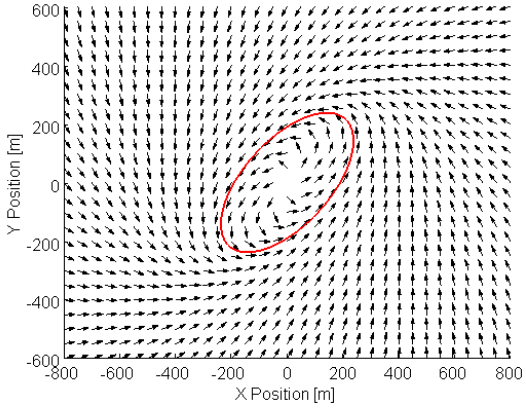

Fig. 5 Elliptical Lyapunov vector field.

Figures 4 and 5 show a single robot tracking the elliptical pattern described above. The robot has speed v_0 = 20 m/s, maximum turn rate ω_{max} = 0.3 rad/s, and initial position [800m, 800m]. Figure 4 shows the path of the robot as it converges to the ellipse. Figure 5 shows the Mahalanobis distance $d_m = \mathbf{x}_r^T P^{-1} \mathbf{x}_r - r_d^2$ as a function of time. The limit cycle behavior is due to the fact that a discrete controller is used with a sample time of 1.0 s and the fact that the desired turn rate $\dot{\psi}_d$ is numerically estimated

$$\hat{\dot{\psi}}_d = \frac{\psi_d\left(\mathbf{x}_r + \Delta t \cdot \left(\alpha \cdot \mathbf{f}\left(\mathbf{x}_r\right) - \mathbf{v}_T\right)\right) - \psi_d\left(\mathbf{x}_r\right)}{\Delta t}. \qquad (15)$$

When the target velocity is known, a correction term is added to the desired relative velocity vector to ensure that the robot remains on the desired contour [1]. We take advantage of the variable scaling factor α in the Lyapunov vector field to recover the commanded speed and retain global convergence as follows. Set the desired inertial velocity of the robot as

$$\begin{bmatrix} u_1 \cos\psi \\ u_1 \sin\psi \end{bmatrix} = \begin{bmatrix} \alpha \cdot \dot{x}_d + T_x \\ \alpha \cdot \dot{y}_d + T_y \end{bmatrix} \qquad (16)$$

where T_x and T_y are the virtual target velocities defined in Section II. Taking the norm of Eq. (16) and setting it to the commanded speed v_o leads to the following expression for

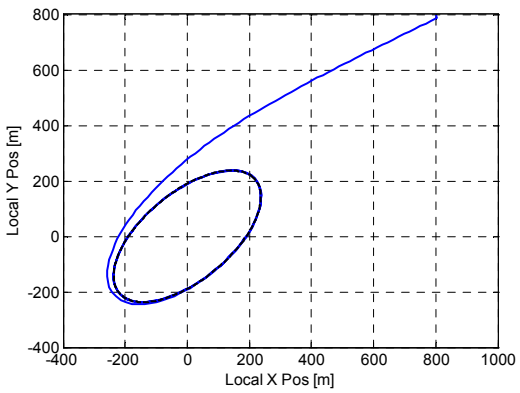

Fig. 3 Path of UA tracking elliptical loiter pattern.

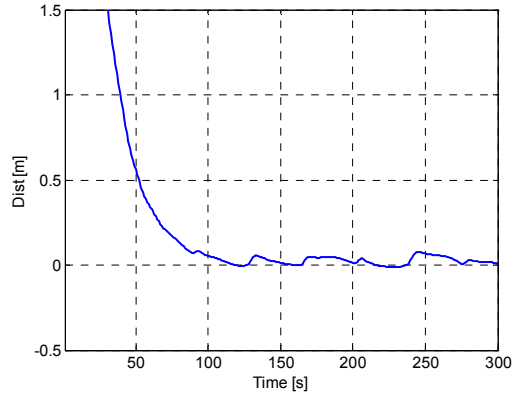

Fig. 4 Mahalanobis distance versus time.

the scale factor:

$$\begin{aligned} &\alpha^2 \cdot \left(\dot{x}_d^2 + \dot{y}_d^2\right) + \alpha \cdot 2 \cdot \left(\dot{x}_d \cdot T_x + \dot{y}_d \cdot T_y\right) \\ &\quad + \left(T_x^2 + T_y^2\right) - v_0^2 = 0 \end{aligned}. \qquad (17)$$

Provided the robot speed v_o is larger than the virtual target speed, Eq. (17) has one positive real solution for α, showing that the scaled vector field remains globally convergent to the loiter circle.

Phase coordination of multiple robots around the desired contour is produced by a second control law, which adjusts the speed of the vehicles (within limits). The resulting speed commands are then processed through the correction algorithm (17) to maintain the desired standoff distance to the moving target. For two cooperating robots with phase angles θ_1 and θ_2 defined relative to the instantaneous target location, the speed commands

$$\begin{aligned} u_{1,1} &= k(\theta_2 - \theta_1 - \theta_D) r_d + v_0 \\ u_{1,2} &= -k(\theta_2 - \theta_1 - \theta_D) r_d + v_0 \end{aligned}. \qquad (18)$$

drive the relative angle $\theta_2 - \theta_1$ to the desired offset θ_D [1].

IV. Tracking An Uncertain Moving Target

In this work we assume either a statistical or set-membership representation of the uncertain moving target. In either representation the uncertain target is given by an

estimate $\bar{\mathbf{x}}_t = [x_t, y_t, \dot{x}_t, \dot{y}_t]^t$ of the target state that includes inertial position and velocity and a matrix $\mathbf{P}$ that describes the uncertainty in the estimate. For the statistical representation the matrix is the estimate error covariance $E\left[(\mathbf{x}-\bar{\mathbf{x}})\cdot(\mathbf{x}-\bar{\mathbf{x}})^t\right]$. The covariance matrix defines hyper-surfaces of constant probability density and can define hyperellipsoidal confidence regions

$$(\mathbf{x}-\bar{\mathbf{x}})^t \mathbf{P}(\mathbf{x}-\bar{\mathbf{x}}) \le n_\sigma^2 \tag{19}$$

where n_σ is a scalar parameter that determines the confidence level. For the set-membership representation the matrix $\mathbf{P}$ is used to define a bounding hyper-ellipsoid around the estimate that contains the true state using (19) with $n_\sigma = 1$.

In order to guarantee stand-off tracking of an uncertain target, a loiter pattern is defined that keeps the robot the specified separation distance r_{off} from the boundary of the bounding position ellipse $\mathbf{P}_p$ defined by the uncertainty matrix:

$$\mathbf{P_p} = E\left[\tilde{\mathbf{p}}\cdot\tilde{\mathbf{p}}^t\right] = \mathbf{P}(1:2,1:2). \tag{20}$$

In order to use the guidance law defined in (10) we calculate the transformation matrix $\mathbf{M}$ from the bounding position ellipse. First, the square root matrix is determined and scaled by n_σ

$$\mathbf{S} = n_\sigma \sqrt{\mathbf{P_p}} = \mathbf{U}\cdot\begin{bmatrix}\sigma_1 & 0\\ 0 & \sigma_2\end{bmatrix}\cdot\mathbf{V}. \tag{21}$$

Next, the singular value decomposition of the resulting matrix $\mathbf{S}$ is calculated. The singular values of $\mathbf{S}$ represent the lengths of the major and minor axis of the bounding ellipse while the orthonormal matrices $\mathbf{U},\mathbf{V}$ define its orientation. The specified stand-off distance is added to each singular value and the transformation matrix $\mathbf{M}$ is created by re-multiplying by the orthonormal matrices to yield

$$\mathbf{M} = \mathbf{U}\cdot\begin{bmatrix}\sigma_1 + r_{off} & 0\\ 0 & \sigma_2 + r_{off}\end{bmatrix}\cdot\mathbf{V}. \tag{22}$$

The net effect is to stretch the bounding ellipsoid by the distance r_{off} in the direction of both axes of the ellipse. The resulting ellipse over-approximates the guaranteed stand-off distance, but is easier to compute from the original bounding ellipse $\mathbf{P}_p$.

V. Simulation Results

Implementation of the guidance law defined by (10), (18), and (22) requires calculation of the full target state. In this paper we use a two step approach. First, measurements for the two robots are combined at each sample time to form an instantaneous estimate of the target position. Second, this estimate is used as the measurement vector for a Kalman filter that estimates the entire target state.

In this work we assume each robot measures the range and bearing to the target. From these measurements, we can invert the measurement function to obtain a local estimate of the target position

$$\hat{\mathbf{p}}_k^i = h^{-1}\left(\mathbf{z}_k^i, \mathbf{x}_k^i\right) \tag{23}$$

and calculate the Cramer-Rao Lower Bound of the position error covariance matrix

$$\mathbf{P}_k^i = \left(\mathbf{H}_k^{i\,t}\cdot\mathbf{R}^{-1}\cdot\mathbf{H}_k^i\right)^{-1} \tag{24}$$

where $\mathbf{H}_k^i$ is the derivative of the measurement function (6) with respect to the target position and $\mathbf{R}$ is the measurement noise covariance matrix.

The measurements from each robot are combined to give the instantaneous position estimate

$$\hat{\mathbf{p}}_k = \hat{\mathbf{P}}_k\cdot\left(\mathbf{P}_k^{1\,-1}\cdot\hat{\mathbf{p}}_k^1 + \mathbf{P}_k^{2\,-1}\cdot\hat{\mathbf{p}}_k^2\right) \tag{25}$$

with new error covariance matrix

$$\hat{\mathbf{P}}_k = \left(\mathbf{P}_k^{1\,-1} + \mathbf{P}_k^{2\,-1}\right)^{-1}. \tag{26}$$

The full target state is then estimated by using $\mathbf{z}_k = \bar{\mathbf{p}}_k$ as the measurement vector with noise covariance $\mathbf{R}_k = \hat{\mathbf{P}}_k$ in a standard Kalman filter.

Simulations were carried out with 2 robots tracking a single moving ground target. The robots start from positions [800m, 800m] and [900m, 890m], have nominal speed v_0=20 m/s with constraints v_{min} = 15 m/s and v_{max} = 25 m/s, and maximum turn rate ω_{max} = 0.2 rad/s. The target starts at the origin and moves with constant velocity [10 m/s, 0 m/s]. The process noise covariance is Q_t = 1.0***I** m/s^2. The range and bearing sensor variances used for the simulation are σ_r = 200 m and σ_θ = 5 degrees. The stand-off distance is r_{off} = 300 m, the sample time is T_s = 1s, and n_σ = 3.

Figures 6-8 show the simulation results. Figure 6a shows the Mahalanobis distance between each robot and the boundary of the instantaneous loiter pattern versus time. Since the uncertainty in the target estimate decreases with time the loiter pattern boundary also changes. Figure 6b shows the separation distance between each robot and the true target location. The robots stay beyond the stand-off distance throughout the entire flight except briefly at approximately 225 s. Figure 6a shows a negative Mahalanobis distance which indicates that the robots were within the boundary ellipse. This tracking error is due to the approximation of the feedforward term given by (15). These results imply that the ellipse given by (22) provides adequate

separation from the uncertain target but that tracking errors can cause the robots to violate the stand-off constraint.

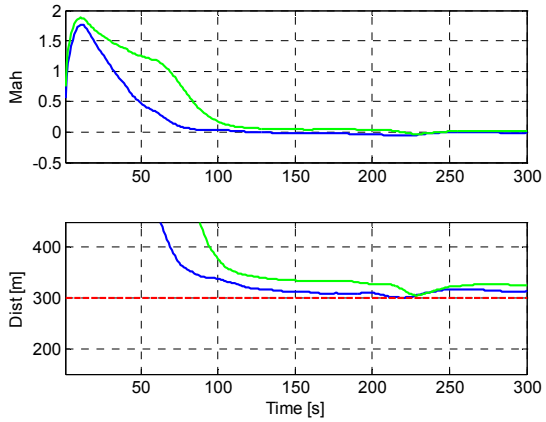

Fig. 6 Lyapunov function and standoff distances versus time for two UA track a moving target.

Figure 7 shows the turning rate and speed commands of the two robots. The turn rate command has high frequency oscillation due to the behavior of the position estimates of the target (Fig. 8). Otherwise, the guidance vector law yields good performance without hitting the turn rate constraints at 0.2 rad/sec. The speed commands also oscillate about the nominal value of 20 m/s. In this case, the oscillation indicates that the vehicles were unable to maintain the desired 90 degree phasing due to the motion of the target.

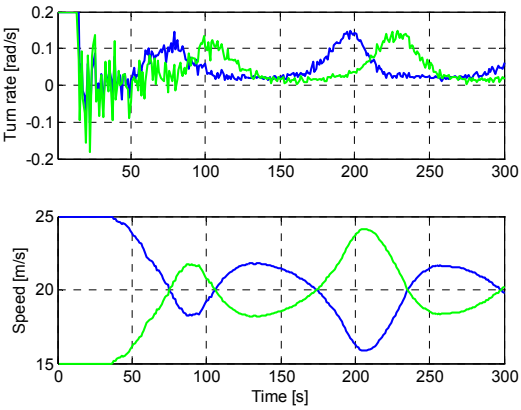

Fig. 7 Two UA track a moving target. Turn rate and speed commands.

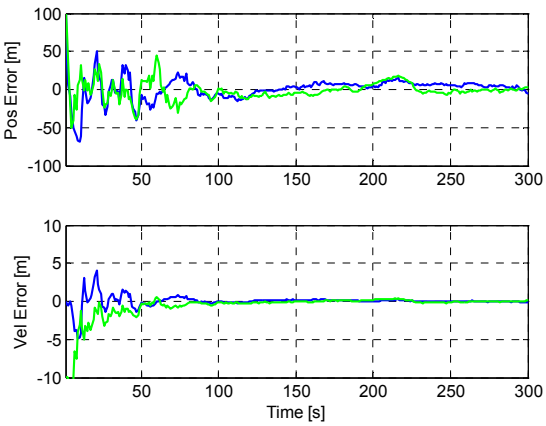

Fig. 8 Two UA track a moving target. Estimator performance.

Figure 8 shows the performance of the target tracking estimation versus time. The position errors initially oscillate with a magnitude of 50 meters but settle in to within 10 meters after 100 s. Likewise, the velocity errors settle to less than 0.5 m/s. Comparing Fig. 8 and Fig. 6 reveals that the estimation performance improves greatly when the robots reach the loiter pattern (Mahalanobis distance close to zero in Fig. 6a) close to the stand-off distance from the target (separation distance close to 300 m).

VI. Conclusion

This paper presented a coordination scheme for standoff tracking of an uncertain moving ground target by two unmanned aircraft. By transforming a circular guidance vector field into elliptical patterns, guaranteed standoff tracking can be achieved that incorporates target uncertainty into the robot motion control. Simulation results demonstrated the ability of two robots to coordinate their orbit around an uncertain target moving with constant velocity.

References

[1] E. W. Frew and D. Lawrence, "Cooperative stand-off tracking of moving targets by a team of autonomous aircraft," in *AIAA Guidance, Navigation, and Control Conference,* 2005.

[2] J. M. Passerieux and D. Van Cappel, "Optimal observer maneuver for bearings-only tracking," *IEEE Trans. Aerospace Electron. Syst.,* vol. 34, pp. 777-788, 1998.

[3] E. Frew and S. M. Rock, "Trajectory generation for monocular-vision based tracking of a constant-velocity target," in *Proceedings of the 2003 IEEE International Conference on Robotics and Automation*.

[4] A. Huster, E. W. Frew and S. M. Rock, "Relative position estimation for AUVs by fusing bearing and inertial rate sensor measurements," in *Oceans 2002 Conference and Exhibition. Conference Proceedings, 29-31 Oct. 2002,* 2002, pp. 1863-70.

[5] A. Makarenko, A. Brooks, S. Williams, H. Durrant-Whyte and B. Grocholsky, "A decentralized architecture for active sensor networks," in *2004 IEEE International Conference on Robotics and Automation,* 26 April-1 May 2004, pp. 1097-102.

[6] D. P. Eickstedt and M. R. Benjamin, "Cooperative target tracking in a dsitributed autonomous sensor network," in *Proc. IEEE/MTS Oceans '06,* 2006.

[7] B. Grocholsky, R. Swaminathan, V. Kumar, C. Taylor and G. Pappas, "Coordinated perception by teams of aerial and ground robots," in *Mobile Robots XVII, Oct 26-28 2004,* 2004, pp. 181-191.

[8] E. W. Frew, J. Langelaan and S. Joo, "Adaptive receding horizon control for vision-based navigation of small unmanned aircraft," in *Proceedings 2006 American Control Conference,* 2006.

[9] J. Ousingsawat and M. E. Campbell, "Establishing trajectories for multi-vehicle reconnaissance," in *Collection of Technical Papers - AIAA Guidance, Navigation, and Control Conference, Aug 16-19 2004,* 2004, pp. 2188-2199.

[10] E. W. Frew, "Sensitivity of cooperative geolocalization to orbit coordination," *Submitted to AIAA Journal of Guidance, Control, and Dynamics,* 2006.

[11] D. Paley, N. E. Leonard and R. Sepulchre, "Oscillator models and collective motion splay state stabilization of self-propelled particles," in *44th IEEE Conference on Decision and Control,* 2005,

[12] R. Rysdyk, C. Lum and J. Vagners, "Autonomous orbit coordination for two unmanned aerial vehicles," in *AIAA Guidance, Navigation, and Control Conference, Aug 15-18 2005,* 2005, pp. 4876-4884.